Rip currents near coastal structures in Lake Michigan: characterization and assessment for warnings

Yuli Liu[a,b] and Chin H. Wu[b]*

[a]School of Marine Sciences, Nanjing University of Information Science and Technology, Nanjing, China

[b]Department of Civil and Environmental Engineering, University of Wisconsin-Madison, Madison, Wisconsin 53706, USA

*Corresponding author: chinwu@engr.wisc.edu

Abstract

Rip currents near coastal structures commonly occur in Lake Michigan in the Great Lakes region of the United States. Lack of timely warning due to undocumented characteristics of rip currents and no assessment tool can contribute to tragic drownings incidents. In this paper, we characterized rip current occurrences near breakwater structures and developed an assessment tool for providing timely rip current warnings to beachgoers at the study site, City of Port Washington, WI. Characteristics of rip currents near the structure were observed from field measurements or visual images. Deflection rip currents had speeds of ~0.2 m/s and lasted for several hours. The rip current occurrences were associated with environmental proxies. It was found that rip currents can occur even when the water appears calm near the structure. A Structure Rip Checklist and Assessment Matrix (SRiCAM) with a four-tiered risk was developed and validated using observations. Furthermore, the SRiCAM was integrated into cyberinfrastructure with a data contingency plan to provide real-time warnings to the public. The applicability of the SRiCAM to other locations across Lake Michigan was further tested and results are promising. Overall, the SRiCAM has the potential to be widely extended to foster recreational water safety and resilience to rip current hazards in the Great Lakes.

Keywords: Rip currents, coastal structure, meteotsunamis, seiches, Lake Michigan

Introduction

Rip currents, which are narrow seaward water jets that can occur adjacent to coastal structures or along beaches, can quickly sweep swimmers into deeper water (Castelle et al., 2016; Dalrymple et al., 2011; MacMahan et al., 2006). Panicked swimmers can become fatigued by trying to swim against rip currents back to shore, leading to drowning (Brander et al., 2011; Davis, 1925; Shepard, 1937). Hundreds of rip-current related drowning incidents have been reported across the world (Arozarena et al., 2015; Brewster et al., 2019; Brighton et al., 2013; Gensini and Ashley, 2010; Short and Hogan, 1994; Woodward et al., 2013). According to the Great Lakes Current Incident Database (GLCID), a total of 703 drowning incidents including 223 fatalities occurred in the Great Lakes region (US/Canada) from 2002-2020. Rip-current related incidents occurred in all the five Great Lakes, and 448 occurred in Lake Michigan (Michigan Sea Grant, 2021). More than 50% of the reported incidents were in the vicinity of coastal structures (Michigan Sea Grant, 2021). In Lake Michigan, 257 coastal structure-related incidents occurred at 38 distinct sites across 18 counties.

On annual average, there were 13 rip current-related incidents near coastal structures in Lake Michigan. A hotspot like the Holland State Park, Michigan had 28 incidents occurred on a single day of August 3, 2011, according to the GLCID. Another hotspot, the Grand Haven State Park, Michigan, had 4 fatalities and 17 rescues caused by structure-related rip currents over the 19 years. While a great amount of progress in documenting rip current hazards has been made over the past decades (Brander and Scott, 2016; Brander and MacMahan, 2011; Castelle et al., 2016; Short and Hogan, 1994), the lack of timely warnings of rip currents near structures can contribute to tragic drowning incidents. In view of the importance and concern, characterizing

and assessing potential occurrences of rip currents near structures would help foster recreational water safety in the Great Lakes (Meadows et al., 2011).

Characteristics of rip currents near coastal structures can be classified into two types (Castelle et al., 2016). First, deflection rip currents occur at the wave-exposed side as offshore-directed flows propagating along the structure (Castelle et al., 2016; Castelle and Coco, 2012; Horta et al., 2018; Scott et al., 2016; van Rijn, 2011). The formation is caused by deflected longshore currents when encountering the rigid boundary (Dalrymple et al., 2011). The speeds of deflection rip currents tend to increase with wave heights and when oblique wave incidence is close to a 45° angle with the shoreline direction (Scott et al., 2016). Deflection rip currents are found to extend far outside the surf zone when the structure is longer than the surf zone width, or when the spacings between two structures (such as in groins or headlands) are 2 to 4 times the lengths (Castelle and Coco, 2013; Scott et al., 2016; van Rijn, 2011). Second, shadow rip currents occur on the lee-wave side as large recirculation eddies (Aelbrecht and Denot, 1999; Gourlay, 1974; Pattiaratchi et al., 2009; Scott et al., 2016; Wind and Vreugdenhil, 1986). The formation of the eddy is caused by differences in radiation stress gradients between the large wave set-ups and the shadowed side of the structure (Gourlay, 1974; McCarroll et al., 2014; Shi et al., 2003). Flow patterns of shadow rip currents have been observed in narrow embayments between headlands (Castelle and Coco, 2013, 2012). Recirculating shadow currents and offshore deflection currents can appear on both ends of the headland boundaries simultaneously. Studies regarding the characterization of rip currents near groins (Aelbrecht and Denot, 1999; Pattiaratchi et al., 2009; Scott et al., 2016) and headlands (Castelle and Coco, 2013, 2012; Gourlay, 1974; Horta et al., 2018) have been well documented. Nevertheless, there are few field measurements of rip currents near structures particularly in the Great Lakes, in comparison with

rip current measurements conducted at beaches (Castelle et al., 2016). Therefore, characterizing rip currents near harbor breakwaters, common coastal structures adjacent to recreation beaches in the Great Lakes, are critically needed.

Assessment of rip current occurrences has been conducted based upon environmental proxies (Dalrymple et al., 2011; Gensini and Ashley, 2010). On oceanic coasts, the Lushine Rip Currents Scale (LURCS) and the modified derivatives are based on causative factors like wind speed and direction, swell height and period, tidal range, and beach morphology (Alvarez-Ellacuria et al., 2009; Arun Kumar and Prasad, 2014; Engle, 2003; Lascody, 1998; Lushine, 1991; Schrader, 2004). In the Great Lakes, the Great Lakes Rip Current Checklist (GLRCC) considers factors like wave height, wave period, wind speed, wind direction, and water level (Meadows et al., 2011). Recently, high-frequency water level oscillation due to storm-induced meteotsunamis (Bechle et al., 2016; Monserrat et al., 2006) and seiches (As-Salek and Schwab, 2004; Rabinovich, 2009), one of the key factors to cause rip currents in open beaches in the Great Lakes (Linares et al., 2019), has further been added to the Flash Rip Occurrence Checklist by Liu and Wu (2019). While a great deal of progress has been made in employing environmental proxies to assess rip currents in open beaches, no tool to assess rip currents near coastal breakwater structures has been reported in the Great Lakes, as far as the authors are aware.

The objective of this paper is to characterize rip current occurrences near breakwater structures and develop an assessment tool for providing timely rip current warnings to beachgoers. Specifically, the occurrences of rip currents were identified and associated with environmental proxies using in-situ measurements and remote imaging observations at the north breakwater of the City of Port Washington, Wisconsin. Pulsating flow characteristics in the

observed rip currents were related to the environmental proxies using wavelet and cross-wavelet analysis. The Structure Rip Checklist and Assessment Matrix (SRiCAM) tool for assessing potential occurrences of rip currents near structures was developed and validated at the study site. Consistent and trustworthy results based upon the SRiCAM were discussed. The SRiCAM tool was integrated into cyberinfrastructure with a data contingency plan to provide reliable and real-time warnings to the public. Lastly, we applied the SRiCAM to other locations around Lake Michigan for assessing rip current hazards near coastal structures to foster coastal community resilience in the Great Lakes.

Methods

Site description

The study site is located on the western shore of Lake Michigan at City of Port Washington, WI. The harbor, representing a typical coastal structure on the Great Lakes, is bound by two concrete breakwaters as shown in Fig. 1. The two breakwaters are 850 meters apart on the land and the two tips are 400 meters apart. The north breakwater has a length of 750 meters and forms an oblique angle of 115° with the shoreline. The south breakwater has a length of 500 m and forms a normal angle with the shoreline. The shoreline is orientated in angle about 30° clockwise from true North. Correspondingly, the shore-normal incidence is 120° from the North. Two recreational beaches, North Beach and South Beach (Fig. 1) are connected to the two ends of the breakwaters. The beach slope is 0.03-0.04 and becomes 0.01-0.015 at offshore distances beyond 100-150 meters from the shoreline. Both beaches are not patrolled by lifeguards. Eight drownings and over ten rescues were reported near the site since 2012,

according to the GLCID (Michigan Sea Grant, 2021) and reports from the Great Lakes Surf Rescue Project (GLSRP, 2021). Specifically, drownings due to rip currents occurred on September 2, 2012 and March 16, 2016 were reported to occur adjacent to the breakwaters of the Port Washington harbor (GLSRP, 2021). While a previous study at the study site (Liu and Wu, 2019) has addressed the flash rips at the North Beach, rip currents near the breakwaters have not been investigated.

Data sources and field measurements

Bathymetry data (Fig. 1) was integrated by combining three sources: nearshore surveyed depths, coastal LiDAR topographic data (Office for Coastal Management, 2014), and NOAA offshore bathymetry of Lake Michigan (National Geophysical Data Center, 1996). The nearshore survey was conducted in 2017 using a Sontek River Surveyor with a 0.5 MHz downward-looking vertical acoustic beam (Lin et al., 2009), with a horizontal resolution of 0.5 meter and a depth resolution of 1 millimeter. The survey covered a nearshore region (2000 m × 250 m) north of the Port Washington harbor. The coastal LiDAR topographic data, which was collected by the USACE NCMP Topobathy Lidar Survey in 2012 (Office for Coastal Management, 2014), covers coastal regions up to 500 meters offshore with horizontal resolutions of 1-3 meters and a vertical resolution of 1 millimeter. The NOAA offshore bathymetry for Lake Michigan has a spatial resolution of 3 geographic seconds. The integrated bathymetry employs unified coordinates based on UTM NAD83 and NAVD88 datums and the overlaid points were averaged using inverse distance weighting.

Meterological data including surface wind speeds, directions, atmospheric pressures, and radar reflectivity images were compiled from multiple sources. First, data at 10-minute interval

was obtained from the NOAA weather station PWAW3 (A1 in Fig. 1) which was established since 2006 as part of the Great Lakes Observation System (GLOS) Weather Station network. Second, 1-minute interval data was collected by a Young ResponseONE Weather Transmitter (A2 in Fig. 2) in 2019 during the swim season deployment at North Beach, which was described in (Liu and Wu, 2019). Third, 1-minute data was obtained from the nearby Automated Surface Observing System (ASOS) at the General Mitchell International Airport in Milwaukee, WI (KMKE, see Fig. 1). Next Generation Radar (NEXRAD) reflectivity images were obtained from the NOAA National Climatic Data Center at 5-minute interval and were used to detect passages of convective storms, which can induce high-frequency water level oscillations like meteotsunamis (Bechle et al., 2015; Linares et al., 2018).

Hydrodynamic data, including nearshore currents, water levels, and wind waves, were measured for a 35-day period from July 27, 2016, to August 31, 2016, and a 10-day period from Aug 9, 2017, to Aug 19, 2017. Nearshore currents on the north side of the Port Washington harbor were measured at three locations (Fig. 1). Two Teledyne RDI Acoustic Doppler Current Profilers (ADCPs) sensors (denoted as C1 and C2 in Fig. 1) were deployed at about 20 meters from the north breakwater at a water depth of 4.6 meters and 6.7 meters, respectively. Profiles of current velocities were sampled at 3 Hz for 2.5 minutes in every 5-minute interval. Farther away from the structure, a Nortek 1 MHz Acoustic Wave and Current Profiler (AWAC) sensor (denoted as CW in Fig. 1) was deployed at a water depth of 5.5 meters. Velocity profiles and wind waves using the acoustic surface tracker technique (Nortek AS, 2005) were sampled in a burst mode of 2 Hz for 8.5 minutes in every 10-minute interval. In addition, an ultrasonic Echologger sensor (denoted as W1 in Fig. 1) was deployed to measure the time series of water surface displacements at 5 Hz.

Visual images at the study site were recorded using a real-time Mobotix 6MP resolution dual-lens camera (Liu and Wu, 2019) on the rooftop of Wastewater Treatment Plant (A2 in Fig. 1). The camera view toward the north side of the breakwater provides a 45°×34° field of view. The camera's central control unit can automatically adjust the brightness to different lighting conditions in a day. High-resolution images were sampled every 5 seconds. The image data were used to detect visual signatures of rip currents such as sediment plumes (Floc'h et al., 2018; Murray et al., 2013) or bubble-laden water jets (Dalrymple et al., 2011; Leatherman and Leatherman, 2017).

Rip current identification

Rip currents were identified based upon directions and magnitudes of measured velocities during the 2016 field measurement. In this study, rip current occurrences were identified using two criteria: (i) velocity direction is within +/- 15 degrees from the angle of the nearby structure (i.e., 145° from the North) toward offshore, and (ii) velocity magnitude is larger than 0.1 m/s, which corresponds to the 95th percentile of measured velocities of the 35-day dataset in 2016. The 0.1 m/s criterion is on the lower end of typical rip current speeds of ~0.4 m/s measured near groins in other studies (Pattiaratchi et al., 2009; Scott et al., 2016). Rip currents of smaller speeds still can pose hazards to weak and non-swimmers (Moulton et al., 2017). The time series of measured current velocities were processed in the following three steps. First, velocity profiles in each sampling interval were averaged over time and water depth. Next, the time and depth-averaged velocities were converted from the universal ENU (East, North, Upward) coordinate system to the location-specific CAU (Cross-shore in x, Alongshore in y, Upward in z) coordinate

system, as shown in Fig. 1 for the x-y plane. Lastly, the calculated velocity magnitudes and directions were checked using the two criteria (i) and (ii).

Rip currents were also identified based upon sediment plumes that appeared in the camera images. To facilitate detection of rip currents, we followed the method of Liu and Wu (2019) to process recorded images in three steps. First, original images in RGB color space are transformed into the HSV color space, which closely resembles human perceived colors. Second, all transformed HSV pixels are partitioned into segments using a k-means clustering method. The regions representing different morphological features, such as the water, the breakwater structure, and rip currents-induced sediment plumes, are separated. Third, images in oblique views are ortho-rectified and transformed into geo-referenced coordinates using parameters obtained from on-site calibration methods (Bechle et al., 2012; Wanek and Wu, 2006). The processed images were checked against the three criteria: (i) pixels in the colors of sediment plumes (Hue<0.167) are detected; (ii) the detected sediment plume in pixel clusters have sizes larger than an area threshold (20 m^2), where the threshold is determined by minimizing any discrepancies between the detections and human eye perceived plumes; and (iii) the centroid locations of detected sediment plumes are in the vicinity of the north breakwater (Liu and Wu, 2019).

Environmental proxies and association

Environmental proxies, like hydrodynamic and atmospheric conditions, were associated with identified rip current events as follows. First, proxies for nearshore hydrodynamic conditions were characterized based upon factors like significant wave height (H_s), peak wave period (T_p), and high-frequency water level fluctuations (HFWLFs, denoted as ΔWL). HFWLFs

were calculated by applying a band-pass filter to isolate water surface displacements with periods less than 2 hours (As-Salek and Schwab, 2004; Bechle et al., 2015; Monserrat et al., 2006). Second, proxies for atmospheric conditions were characterized based upon factors like wind speeds (W_s), wind directions (Dir_w), wind shifts (ΔDir_w) and pressure disturbances (ΔP). Wind directions were measured as the angle clockwise from true North and were reported in the sixteen-wind compass. Wind shifts were calculated as the wind direction changes in degrees per hour. Pressure disturbances (ΔP) were calculated from filtered air pressures using a 2-hour cut-off period. In addition, a proxy for convective storm was characterized by detecting storm structures in radar reflectivity images (Bechle et al., 2015). The storm proxy was included in this study because storm-induced atmospheric disturbances are common drivers of HFWLOs like seiches and meteotsunamis that can propagate as edge waves (Bechle et al., 2014), affect nearshore hydrodynamics (Bechle et al., 2015) and cause rip currents (Linares et al., 2019).

Wavelet analysis

Wavelet analysis is capable of simultaneously revealing the time and frequency features of time series signals. Wavelet analysis (Daubechies and Sweldens, 1998; Torrence et al., 1998) has been employed in studies of nearshore processes, such as rip channel evolutions (Barrett and Houser, 2012), wave breaking patterns (Liu and Babanin, 2004), and high-frequency water level fluctuations (Linares et al., 2016). In this study, we employed a Morlet mother wavelet function (Torrence et al., 1998) to calculate wavelet power spectra (WPS) of current speeds measured by the three sensors (C1, C2, and CW). Velocity pulsations in rip current events were characterized based upon calculated WPS. To examine causative relationships of occurrences and pulsating behaviors of rip currents with environmental proxies, cross-wavelet spectrum analysis (Grinsted

et al., 2004) was employed. Specifically, cross-wavelet power spectra (CWPS) of rip current speeds and water levels, speeds and wind speeds, speeds and air pressures were calculated, respectively. The CWPS were normalized against red noise above the 95% confidence level to isolate common power between the two signals that are statistically significant. In short, wavelet and cross-wavelet analysis were included to provide additional frequency information for characterizing the occurrences and the environmental proxies of rip currents near coastal structures.

Structure Rip Checklist and Assessment Matrix (SRiCAM)

A new tool, based on the Great Lakes Rip Current Checklist (GLRCC; Meadows et al., 2011) and incorporating additional environmental proxies, was developed to assess rip current occurrences near coastal structures. Table 1 shows that four factors (i.e., wave height, wave period, wind speed, and lake level) were adopted from GLRCC (Meadows et al., 2011). We adjusted the wave period factor to account for wind fetches at the study site. Five new factors including wind direction, high-frequency water level fluctuation, wind shift, pressure disturbance, and visual image were added. Points from each factor that meets the corresponding criterion in the SRiCAM are added to yield a total point (*TP*). The potential occurrence of rip currents is assessed based upon *TP* into four risk tiers: *very high* ($TP > 11$), *high* ($11 \geq TP > 7$), *moderate* ($7 \geq TP \geq 4$), and *low* ($4 > TP > 0$). At a *very high*-risk tier, rip currents will occur and can impose life-threatening hazards to people who are close to the breakwater. At a *high*-risk tier, rip currents are expected to occur and can be dangerous near the breakwater. At a *moderate*-risk tier, rip currents are possible to occur near the structure. At a *low*-risk tier, rip currents are generally not expected.

Results

Rip current characteristics

Fig. 2 shows the time series of the measured current speeds and directions near the north breakwater. Fourteen events of rip currents were identified as the measured velocities exceeded the threshold of 0.1 m/s at either the C1 or the C2 location. The events are highlighted by shaded rectangles in Fig. 2 and are numbered chronologically. Each event is denoted with a letter *I* (increasing) if the speeds at C1 were smaller than the speeds at C2, or with a letter *D* (decreasing) if otherwise. Table 2 summarizes the maximum rip speeds (U_{max}) and the durations (ΔT), and the forms of increasing or decreasing currents for each event. The speeds of the identified rip currents were between 0.10 – 0.23 m/s and the durations were between 1.7 – 27.1 hours. Eight rip events (1, 3, 4, 6, 7, 8, 11, and 14) with an average speed of 0.13 m/s and an average duration of 7.1 hours exhibited as the *I*-form currents. The other six events (2, 5, 9, 10, 12, and 13) with an average speed of 0.10 m/s and an average duration of 3.1 hours exhibited as the *D*-form currents. Rip current feeding flows were measured at CW located farther away from the breakwater. The currents at CW were on the same order of magnitude as the rip currents at C1 and C2, but the directions were mostly alongshore. The current directions passing CW were southward (averagely ~ 190° clockwise from true North) for the *I*-form currents and southwestward (~213°) for the *D*-form currents. Note that for the *I*-form currents, the angle between the longshore currents and the orientation of north breakwater (see Fig. 1) is approximately 45°, coinciding with an optimum angle for currents to deflect offshore along the breakwater (Scott et al., 2016). The average speeds and the durations of events with the *I*-form

currents tended to be larger and longer than events with the *D*-form currents. Overall, two forms of rip currents near the breakwater, along with the longshore feeding currents of similar speeds, were characterized.

Velocity pulsations measured by the three sensors at C1, C2, and CW during the fourteen identified rip current events are evident in Fig. 3, which shows the wavelet power spectra (WPS) of current speeds normalized against the variance in log scaled color contours. The black lines represent WPS at the 95% confidence level and the bounded regions were considered as statistically significant. High energy pulsations at periods between 60 and 120 minutes were evident with the WPS>1 at all three locations. Particularly, pulsations of so-called Very Low Frequencies (VLFs), defined as currents with periods <30 minutes (MacMahan et al., 2010) or frequencies <4.0 mHz (Elgar and Raubenheimer, 2020), were found statistically significant at C1 (events 2, 4, 9, 10 and 14) and C2 (events 9, 10, 11 and 12). The velocities of the VLF pulsations, isolated by bandpass filtering, were in the range of 0.04-0.07 m/s and contributed up to ~70% (event 11) of the rip current velocities. In comparison, the VLF pulsations were less obvious at CW. The finding suggests that the VLF pulsations can be a key component contributing to the rip current speeds and may not be caused by the longshore feeding currents.

Environmental proxies for rip current occurrences

Four environmental proxies, based on factors of nearshore significant wave heights (H_s), wave periods (T_p), wind speeds (W_s), and wind directions (Dir_w), were associated with identified rip current events, as shown in Fig. 4 (a-b). The first (I) was characterized by high waves and N-E winds and was associated with events 1, 2, 4, 11, and 14 (Table 2). Significant wave heights were larger than 0.45 meter with the peak wave periods above 4 seconds. Winds with an average

speed of 5.1 m/s were from N to E directions. Wave-driven longshore currents flowed toward the structure to form deflection rip currents. The second (II) was characterized by moderate to low waves (H_s>0.15 m) and N winds (Dir_w < 45°) and was associated with events 3, 6, 7, 8, and 10. Wind waves in highly oblique incidence or wind stress parallel to the shoreline (~ 30°) induced longshore currents toward the breakwater to generate deflection rip currents. The third (III) was characterized by high waves and S winds and was associated with event 9. With significant wave heights as high as 0.84 m at CW, wave-induced currents formed shadow rip currents on the north side (downdrift) of the breakwater. The fourth (IV) was characterized by wind direction shifts (ΔDir_w>15°/hour) and low waves (H_s<0.15 m) and was associated with events 5, 12, and 13. Note that low-wave conditions are unlikely for wave-driven rip currents to form, but the wind shifting possibly created a transient forcing to cause temporary rip currents near the breakwater. The durations of rip currents in the events associated with proxy IV were observed to be relatively short (ΔT <2 hours), in comparison with the other events (Table 2).

Three additional environmental proxies were based on new factors such as high-frequency water level fluctuations (ΔWL), atmospheric pressures disturbances (ΔP), and storm structures related to identified rip currents. The new factors were included to address meteorologically induced water level fluctuations, a new cause of rip currents near structures in a recent study by Linares et al. (2019). The fifth (V) proxy was characterized by ΔWL larger than the standard deviation (σ = 0.04 meter) and was associated with the majority (10 out of 14) of events (Fig 4 c). During events 6 and 11, water level oscillations reached $\Delta WL > 2\sigma$ and relatively large rip speeds were observed (>0.15 m/s; Table 2). The sixth (VI) was characterized by atmospheric pressure disturbances (ΔP >~ 0.5 hPa) during or before rip currents and were associated with events 1, 5, 6, 9, 10, and 13 (Fig 4d). Nevertheless, proxies V and VI were

associated with the days of 2016/08/04, 2016/08/17, and 2016/08/19 (Fig 4c, d) without rip currents (Fig. 2). One possible reason was that the water level fluctuations (proxy V) might be infra-gravity waves (Bertin et al., 2018), not in the same form to cause rip currents near structures as the meteorologically induced water level fluctuations described by Linares et al. (2019). Another possibility was that the pressure perturbations (proxy VI) and the induced water level fluctuations (proxy V) hit the shoreline at normal incidence and did not generate longshore currents to form deflection rip currents along the breakwater structure. The seventh (VII) proxy was characterized by storm structures (Bechle et al., 2015) and was associated with 9 events (Table 2).

Environmental proxies were further associated with velocity pulsations in identified rip current events. Fig. 5 (a), (b), and (c) show the normalized cross-wavelet power spectra (CWPS) of the observed current velocities at C2 and water levels, atmospheric pressures, wind speeds, respectively. Based on the energetic CWPS shown in Fig. 5, we observed that the rip currents pulsated at similar periods as water levels and atmospheric factors, further supporting the association between the environmental proxies with the rip current events. Particularly, significant common power (normalized CWPS>1) was observed at periods <30 minutes, suggesting that the VLFs, a key component of rip velocities (Fig. 3), were associated with or even caused by the environmental proxies. The results based upon CWPS analysis support the previous finding that atmospheric disturbances (proxies IV, VI, VII) or/and induced water level fluctuations (proxy V) can lead to dangerous rip currents near structures (Linares et al., 2019).

To sum up, based on the time series (Fig. 4) and the cross-wavelet analysis (Fig. 5), the identified deflection or shadow rip currents were associated with the seven environmental proxies. Proxies I and III were characterized by high waves and favorable wind directions. Proxy

II was characterized by shore-parallel winds (Scott et al., 2016). Proxy IV was characterized by shifting winds. Proxies V, VI, and VII were characterized by high-frequency water level oscillations, atmospheric pressure disturbances, and convective storm structures, respectively (Linares et al., 2019; Liu and Wu, 2019). Furthermore, most occurrences (12 out 14; Table 2) and velocity pulsations were associated with more than one environmental proxy during a rip current event. The framework of using multiple (seven) proxies allowed us to best characterize rip current near structures under a broad range of possible causative conditions, which would be additional factors of the Great Lakes Rip Current Checklist (Meadows et al., 2011).

Visual signatures of rip currents

Visual signatures of rip currents (i.e. sediment plumes) were captured by the camera A2 (Fig. 1). Fig. 6 shows four example images of rip current events. Patterns of rip-current induced sediment plumes in the four events (1, 3, 9, 5) were different. In event 1 (Fig. 6a), a plume patch appeared near the north breakwater without apparent feeding longshore currents. In event 3 (Fig. 6b), noticeable longshore currents were deflected to generate a narrow band of rip-current induced sediment plumes along the breakwater. In event 9 (Fig. 6c), a patch of plumes due to longshore feeding currents was apparent, but no deflection rip current was visible along the breakwater. In event 5 (Fig. 6d), the water appeared calm with no sediment plume, while the velocity measurements at C1 captured offshore rip currents up to 0.16 m/s (Table 2). The example of Fig. 6 (d) suggests that rip currents near structures can be a hidden hazard to those who are unaware. Events 1, 9, and 5 were associated with storm-related proxies V, VI, and VII, respectively, inferring that cloudy weather (Fig. 6a, c, and d) also can be used as a visual proxy of rip currents. Note that event 3 was associated with a cluster storm (proxy VII). The storm

crossed southern Lake Michigan without passing the study site, but the induced water level oscillation might still affect the site by propagating as edge waves along lake coasts (Linares et al., 2019). The weather (Fig. 6b) appeared sunny and the danger of rip currents was disguised. Overall, visual signatures of sediment plumes can directly provide vivid evidence of rip currents. When there is no apparent sediment plume near the structure, environmental proxies can be used to assess potential occurrences of hidden rip currents near coastal structures.

Evaluation of SRiCAM

The five new factors added to the SRiCAM (Table 1) are rationalized here. The wind direction factor accounts for proxies I and II for deflection rip currents ("updrift") and proxy III for shadow rip currents ("downdrift"). As rip currents associated with proxies I and II were more frequently observed, two points were assigned to the "updrift" criteria in Table 1. The wind shift factor addresses proxy IV for rip currents due to transient wind forcing. The high-frequency water level fluctuation factor addresses proxy V for rip currents due to meteotsunamis (Linares et al., 2019) or seiches (Meadows et al., 2011). The pressure disturbance factor addresses proxy VI for rip currents with dangerous pulsating velocities. Lastly, a visual image factor addresses two situations: (i) proxy VII for rip currents related to storm structures (Linares et al., 2019) and (ii) direct visual signatures of rip currents (i.e. sediment plumes).

Outcomes of the SRiCAM assessing rip current occurrences near the north breakwater were evaluated. Table 3 shows 22 rip current events including the 14 events in 2016. Additional 8 events were identified based on velocity measurements conducted from Aug 9 to Aug 19, 2017 (denoted as "Velocity" in Table 3) or visual evidence of rip currents imaged by the A2 camera in 2017-2019 (denoted as "Image"). All the events were assessed in the *moderate-*, *high-*, or *very*

high-risk tier. The contributions from the five new factors were 75% on average for all events. For events assessed in the *very high*-risk tier (1, 16, 18, 20, 21), the contributions from the new factors were in the range of 70-80%, which were associated with proxy I and proxies V, VI, VII. For events assessed in the *high*-risk tier (2, 3, 9, 19, 22), the new factor contributions exhibited large variations from 56% (in event 19) to 95% (in event 22). For events assessed in the *moderate*-risk tier, large variations in the new factor contributions also were noticed. For example, a low 50% contribution from the new factors in event 14 was associated with proxy I. A high 91% contribution from the new factors in event 5 was associated with proxies IV, V, VI, VII (see Table 2). In short, the new factors added to the SRiCAM reflect important contributions. In addition, 9 out of 10 events assessed in the *very high*- or *high*-risk tier were also identified by visual evidence of sediment plumes, supporting the effectiveness of the new visual image factor to reflect associated risks. Overall, the SRiCAM was developed and validated. The new assessment tool can effectively provide warnings for potential occurrences of rip currents near the breakwater.

Discussion

Multi-tiered risk assessments

Four- and three-tiered risk assessments are compared and discussed here. The four-tiered SRiCAM is compared with a three-tiered version, which assesses $TP \geqslant 5$ in a *moderate*-risk tier and $TP \geqslant 10$ in a *high*-risk tier. For a hidden rip current event such as event 7, the *TP* was 4.5, yielding a *moderate* risk based upon the four-tiered version. In comparison, the three-tiered assessment would give a *low* risk. Similarly, 5 out of the 12 events in the *moderate*-risk tier

(four-tiered assessment), would be assessed in the *low*-risk tier if using the three-tiered version. Furthermore, event 19 in the *high*-risk tier (four-tiered assessment) would be assessed in the *moderate*-risk tier if using the three-tiered version. In other words, the three-tiered risk assessment tends to underestimate risks, resulting in low trust to the public (Houser et al., 2019).

We further compare the four-tiered SRiCAM with the three-tiered GLRCC. By incorporating new proxy factors and building upon the weighting of original GLRCC factors for wind wave-driven rip currents in open beaches (Meadows et al., 2011), the SRiCAM is capable of addressing rip currents near structures. Under wind waves dominating conditions (proxies I, III), the SRiCAM adds points contributed from original factors in the GLRCC, yielding consistent assessments. Under mixed conditions such as strong shore-parallel winds (proxy II), shifting winds (proxy IV), meteorologically induced (proxies VI, VII), or water level fluctuations (proxy V) including meteotsunamis and seiches (Linares et al., 2019; Meadows et al., 2011), the SRiCAM considers significant contributions (>50%, see Table 3) from new factors to capture hidden rip currents, which would otherwise be assessed as low-risk by the GLRCC. In recent years, four-tiered risk assessments have been adopted by several rip current warning systems, such as by Arun Kumar and Prasad (2014) and by the National Weather Service (Grand Rapids Michigan) on July 10, 2020 via Facebook (https://www.facebook.com/NWSGrandRapids/). Overall, the four-tiered risks in the SRiCAM shows trust-worthy and consistent assessments of potential rip currents occurring near coastal breakwater structures.

Integration of cyberinfrastructure

Cyberinfrastructure technology has been widely employed to provide real-time hazard-related warnings in recent years. In this study, the SRiCAM has been integrated into Integrated Nowcast Forecast Operation System developed for the Great Lakes region (Anderson and Wu, 2018; Liu and Wu, 2019; Reimer and Wu, 2016), in order to provide real-time warnings of rip currents near the north breakwater at City of Port Washington, WI (URL: https://infosportwashington.cee.wisc.edu/Northbreakwaterwatch1.html). Fig. 7 shows the webpage during the rip current event 22 on 2019/08/15 at 15:25 PM as an example. On the top of the page, the assessment of a *high*-risk tier is highlighted, and the text is designed to change accordingly based upon four risk tiers. Underneath appears detailed information about rip currents in three columns. On the left column, the total points and the SRiCAM are shown. Particularly, the explanations for "*very high*", "*high*", "*moderate*", "*low*" risks are provided, and the suggested actions are emphasized for each risk tier. The wordings were adapted from the local signage provided by the City of Port Washington (Liu and Wu, 2019) and forecast descriptions provided by the NOAA National Weather Service (https://www.weather.gov/safety/ripcurrent-forecasts). In the middle column, current conditions of the nine SRiCAM factors are shown. On the right column, a webcam image shows rip-induced sediment plumes. Lastly, safety education is incorporated at the right bottom corner. The message of "Be Cautious on Both Sides of Breakwater!", a schematic of deflection and shadow rip currents occurring at the same time (Scott et al., 2016), and additional safety messages are provided. Overall, integration of the SRiCAM into the cyberinfrastructure provides real-time warnings of rip current hazards near coastal structures in the Great Lakes for the first time, as far as the authors are aware.

Data contingency plan

Reliable real-time assessment for hazard-related risks requires a data contingency plan (Anderson and Wu, 2018). During temporary station downtime or seasonal sensor unavailability, environmental factors like wave height, wave period, wind speed, wind direction, and pressure disturbance, or water level fluctuations cannot be accounted for. The contingency plan was designed to stream in data from nearby stations to avoid spurious low total points and underestimated risk assessment. Specifically, wave information can be obtained from two wave buoys: (i) NDBC station 45013 at Atwater Park, located 20 miles south of Port Washington harbor, and (ii) NOAA station 45007 in central South Lake Michigan. Additional meteorological wind and atmospheric pressure data are obtained from three stations: NDBC stations MLWW3 at Port of Milwaukee, SGNW3 at Sheboygan, and an Automated Weather Observing System (AWOS III) station KETB at West Bend to further augment observations at NDBC station PWAW3 and ASOS station KMKE. Water level oscillations can be obtained from the NOAA gauge (9087057) in Milwaukee.

Two-step data contingency procedures are executed as follows to ensure that all factors are counted. In step (I), alternative observations from nearby sensors are used to replace the missing data. Nearshore waves at the study site are estimated by adjusting offshore wave observations through the linear-wave dispersion relation (Dean and Dalrymple, 1991). The water level fluctuations criteria are adjusted to station-specific thresholds determined in previous meteotsunami studies (Bechle et al., 2016, 2015, and Linares et al., 2016). In step (II), outputs from the Great Lakes Coastal Forecasting System (GLCFS), downloaded from the GLOS Thredds Server (http://tds.glos.us/thredds/catalog/catalog.html) for gridded wind, pressure, and

wave fields, are used if no alternative observation is available from step (I). The GLCFS, developed by the Great Lakes Environmental Research Laboratory (Alves et al., 2014; Liu et al., 1984; Schwab et al., 1984), is operated to provide real-time nowcasting/forecasting of hydrodynamic condition across the Great Lakes. In short, the data contingency plan is essential to provide reliable warning messages of rip current occurrences near the breakwater structure.

Applicability to other locations in Lake Michigan

Applicability of the SRiCAM to other locations near harbor breakwaters around Lake Michigan was examined. Assessments were based on observation data in Lake Michigan from multiple sources including 12 NDBC offshore wave buoys for wave factors, 20 NDBC and ASOS weather stations for winds and pressure factors, and 10 NOAA water level gages for high-frequency water level fluctuation factor. Specifically, nearshore waves were estimated using the dispersion relation (Dean and Dalrymple, 1991). Observed wind directions were compared against shoreline and structure orientations at each location to determine the "updrift" or "downdrift" factor. Fig. 8 (a) shows an example of applying the SRiCAM to assess risks of rip currents on 2019/07/20 at 39 locations in Lake Michigan including Port Washington, WI. The majority (27 out of 39) of locations were assessed as being at *moderate* risk, 10 at *high* risk, and 2 at *low* risk. The assessed risk tiers were consistent with the visual images of rip current occurrences at three locations spanning across the west, south, and east coasts of Lake Michigan at Port Washington, WI ([1]; Fig. 8b), Michigan City, IN ([14]; Fig. 8c), and Grand Haven, MI ([21]; Fig. 8d), respectively. In the three images, rip-induced sediment plumes, shown as red arrows in Fig. 8 (b, c, d), were captured by the camera A2 at the study site (Fig. 1), a webcam by the Great Lakes Meteorological Real-Time Coastal Observation Network and an EarthCam

(earthcam.com), respectively. Note that the image of Fig. 8 (e) shows choppy water without apparent sediment plumes at South Haven ([17]). The assessment was a *moderate* risk, suggesting that there were possible hidden rip currents near the breakwater. In some cases, the assessment outcomes were not yet certain. The assessment for Sheridan Park ([8]) and Chicago, IL ([9]), two locations close to each other, were a *moderate* risk (*TP*=5) and a *low* risk (*TP*=2), respectively. Further study is needed to adjust the environmental proxies in the SRiCAM to the risk tier due to differences in site-specific conditions and local structure configurations. Overall, applicability of the SRiCAM in assessing potential rip current occurrences at locations near harbor breakwaters in Lake Michigan is promising. Future work should be devoted to incorporating and integrating the SRiCAM into regional cyberinfrastructures like the Great Lakes Beach Hazards (National Weather Service, NOAA, 2020) for providing real-time warnings for rip currents near harbor breakwaters in the Laurentian Great Lakes.

Visual identification

Visual identification of rip current based on induced sediment plumes is discussed. In this study, 9 out the 22 events were identified based on images (Table 3). Signatures of sediment plumes tended to appear under two situations. First, sediment plumes were observed in events during or after convective storms crossing the lake (proxy VII). Sediments, possibly from lake bottom at shallow depths near the shoreline, may be stirred up by high-frequency water level fluctuations (proxy V) caused by storm disturbances (proxy VI). Second, plumes with longshore deflection trajectories (such as in Fig. 6b and Fig 7) were commonly observed under highly oblique incidence waves or shore parallel winds (proxy II). Sediments, possibly from the North Beach and the connected bluff, can be carried by wave- or wind-induced longshore currents toward the breakwater and deflection rip currents. Furthermore, by estimating the rip length

(~750 m) in Fig. 7 using the transformation method (Bechle et al., 2012; Wanek and Wu, 2006) and tracking plume propagations over multiple images, the speed of rip currents was estimated to be 0.2 m/s, similar to measured rip velocities (Table 2). Overall, visual identification based on sediment plumes was illustrated at the study site (Fig. 6, 7) and at other locations across Lake Michigan (Fig. 8), suggesting that image observation can be widely applied to direct reflect rip current risks near coastal structures.

Summary and Conclusions

Rip currents at the study site near the north breakwater of City of Port Washington, WI were characterized. Occurrences of rip currents were identified using field measurements of current velocities and image observations. Hidden dangers of rip currents near coastal structures were illustrated in images, velocity time series, and wavelet analysis. There were three findings. First, rip currents near the north breakwater were usually accompanied by strong longshore currents that can carry unalerted swimmers into the hazardous offshore flows. Second, environmental proxies of rip current occurrences near coastal structures include traditional factors such as wave height, wave period, wind speed, and lake level, and new factors such as wind direction, wind shift, atmospheric pressure disturbance, high-frequency water level oscillation, and visual image that have not been incorporated before. Third, rip currents can still be present near coastal structures when the water appears seemingly safe with no apparent visual signatures. Overall, rip currents near the breakwater structures were characterized and associated with environmental proxies in Lake Michigan for the first time.

A Structure Rip Checklist and Assessment Matrix (SRiCAM) tool was developed and validated at the study site. The SRiCAM is an environmental proxy-based tool for assessing rip current occurrences near coastal structures. Particularly, the SRiCAM uses factors to address less- recognized environmental proxies including strong shore-parallel winds, shifting winds, and atmospheric pressure disturbances, meteorologically induced water level fluctuations like meteotsunamis and seiches, and storm structures. Four-tiered risk assessments were employed to faithfully assess potential rip currents near coastal structures. With the integration of the SRiCAM into the cyberinfrastructure and the implementation of a data contingency plan, real-time rip current warnings can be reliably provided to the public. Applicability of the SRiCAM to 39 locations near harbor breakwaters around Lake Michigan is promising. Overall, the SRiCAM can be widely extended to larger regions of the Great Lakes in the future to foster the resilience of coastal communities to rip current hazards.

Declaration of Competing Interest

The authors declare that they have no known competing financial interests or personal relationships that could have appeared to influence the work reported in this paper.

Acknowledgments

This study was supported by the Wisconsin Coastal Management Program (WCMP), National Oceanic and Atmospheric Administration (NOAA) Coastal Storms Program, University of Wisconsin Sea Grant Institute (UW-Sea Grant), and gift funds from WE Energies and local friends of Port Washington group. We would like to thank Mr. Todd Breiby, Ms. Angel Kathleen, and Mr. Michael Friis, from WCMP for the support, coordination, and outreach of rip current safety. In addition, Ms. Moira Harrington at UW-Sea Grant for her dedication to communicating rip current hazards to the Great Lakes community is acknowledged. Outreach activities related to the NOAA rip current outlook by Mr. Marc Kavinsky, Lead Forecaster of Marine Program at NOAA-National Weather Service – Milwaukee/Sullivan, are noted. Mr. Jon Crain and Ms. Kiley Schulte, Mr. Dennis Cherny, Mr. Dan Buehler, and many staff at the City of Port Washington, WI, and Mr. Michael Diemer and Mr. Tom Phelps at DigiCorp INC for the assistances in real-time field measurements acknowledged. Last but not least, the authors especially thank Mr. Tom Mlada, Marty Becker, and Ted Neitzke IV, former Mayors and current Mayor of City of Port Washington, respectively, for their support to emphasize the importance of providing rip current warning for beach safety. Insightful comments and valuable suggestions provided by three anonymous reviewers and editors are highly appreciated and acknowledged.

References

Aelbrecht, D., Denot, T., 1999. 2D and 3D modelling of wave-driven currents in presence of a groin system in a tidal sea, in: Brebbia, C.A., Anagnostopoulos, P. (Eds.), Coastal Engineering and Marina Developments. WIT Press, Southampton, 35–44.

Alvarez-Ellacuria, A., Orfila, A., Olabarrieta, M., Gómez-pujol, L., Medina, R., Tintoré, J., 2009. An alert system for beach hazard management in the balearic islands. Coast. Manag. 37, 569–584. https://doi.org/10.1080/08920750903150662.

Alves, J., Chawla, A., Tolman, H., Schwab, D., Lang, G., Mann, G., 2014. The operational implementation of a Great Lakes wave forecasting system at NOAA/NCEP. Weather Forecast. 29. https://doi.org/10.1175/WAF-D-12-00049.1.

Anderson, J. D., Wu, C. H., 2018. Development and application of a real-time water environment cyberinfrastructure for kayaker safety in the Apostle Islands, Lake Superior. J. Great Lakes Res. 44, 990–1001. https://doi.org/10.1016/J.JGLR.2018.07.006

Arozarena, I., Houser, C., Echeverria, A.G., Brannstrom, C., 2015. The rip current hazard in Costa Rica. Nat. Hazards 2, 753–768.

Arun Kumar, S.V.V., Prasad, K.V.S.R., 2014. Rip current-related fatalities in India: a new predictive risk scale for forecasting rip currents. Nat. Hazards 70, 313–335.

As-Salek, J. A., Schwab, D. J., 2004. High-frequency water level fluctuations in Lake Michigan. J. Waterw. Port Coastal Ocean Eng. 130(1), 45–53.

Barrett, G., Houser, C., 2012. Identifying hotspots of rip current activity using wavelet analysis at Pensacola Beach, Florida. Phys. Geogr. 33, 32–49. https://doi.org/10.2747/0272-3646.33.1.32

Bechle, A.J., Kristovich, D.A.R., Wu, C.H., 2015. Meteotsunami occurrences and causes in Lake Michigan. J. Geophys. Res. Ocean. 120, 8422–8438.

Bechle, A.J., Wu, C.H., 2014. The Lake Michigan meteotsunamis of 1954 revisited. Nat. Hazards 74 (1), 155–177. https://doi.org/10.1007/s11069-014-1193-5.

Bechle, A.J., Wu, C.H., Kristovich, D.A.R., Anderson, E.J., Schwab, D.J., Rabinovich, A.B., 2016. Meteotsunamis in the Laurentian Great Lakes. Sci. Rep. 6, 37832. https://doi.org/10.1038/srep37832

Bechle, A.J., Wu, C.H., Liu, W.-C., Kimura, N., 2012. Development and Application of an Automated River-Estuary Discharge Imaging System. J. Hydraul. Eng. 138, 327–339. https://doi.org/10.1061/(ASCE)HY.1943-7900.0000521

Bertin, X., De Bakker, A., Van Dongeren, A., Coco, G., André, G., Ardhuin, F., Bonneton, P., Bouchette, F., Castelle, B., Crawford, W.C., Davidson, M., Deen, M., Dodet, G., Guérin, T., Inch, K., Leckler, F., Mccall, R., Muller, H., Olabarrieta, M., Roelvink, D., Ruessink, G., Sous, D., Stutzmann, É., Tissier, M., 2018. Infragravity waves: From driving mechanisms to impacts. Earth-Science Rev. 177, 774–799. https://doi.org/10.1016/j.earscirev.2018.01.002

Brander, R. W., Bradstreet, A., Sherker, S., MacMahan, J., 2011. The behavioural responses of swimmers caught in rip currents: new perspectives on mitigating the global rip current hazard. Int. J. Aquat. Res. 5, 476–482.

Brander, R.W., MacMahan, J.H., 2011. Future challenges for rip current research and outreach, in: Leatherman, S., Fletemeyer, J. (Eds.), Rip Currents: Beach Safety, Physical Oceanography, and Wave Modeling. CRC Press, Boca Raton, 1–29.

Brander, R. W., Scott, T., 2016. Science of the rip current hazard, in: Tipton, M., Wooler, A. (Eds.), The Science of Beach Lifeguarding: Principles and Practice, CRC Press, Boca Raton, 67–85.

Brewster, B.C., Gould, R.E., Brander, R.W., 2019. Estimations of rip current rescues and drowning in the United States. Nat. Hazards Earth Syst. Sci., 19(2), 389–397. https://doi.org/10.5194/nhess-19-389-2019

Brighton, B., Sherker, S., Brander, R., Thompson, M., Bradstreet, A., 2013. Rip current relat- ed drowning deaths and rescues in Australia 2004–2011. Nat. Hazards Earth Syst. Sci. 13, 1069–1075.

Castelle, B., Coco, G., 2012. The morphodynamics of rip channels on embayed beaches. Cont. Shelf Res. 43, 10–23.

Castelle, B., Coco, G., 2013. Surf zone flushing on embayed beaches. Geophys. Res. Lett. 40, 2206–2210.

Castelle, B., Scott, T., Brander, R. W., McCarroll, R. J., 2016. Rip current types, circulation and hazard. Earth Sci. Rev. 163, 1–21. https://doi.org/10.1016/J.EARSCIREV.2016. 09.008.

Dalrymple, R. A., MacMahan, J. H., Reniers, A. J. H. M., Nelko, V., 2011. Rip currents. Annu. Rev. Fluid Mech. 43, 551–581. https://doi.org/10.1146/annurev-fluid-122109- 160733.

Daubechies, I., Sweldens, W., 1998. Factoring Wavelet Transforms into Lifting Steps. J. Fourier Anal. Appl. 4, 247–269. https://doi.org/10.1007/bf02476026

Davis, W.M., 1925. The undertow myth. Science. 61, 206–208.

Dean, R.G., Dalrymple, R.A., 1991. Water Wave Mechanics for Engineers and Scientists, Advanced Series on Ocean Engineering: Volume 2. World Scientific Publishing Company, Toh Tuck Link, Singapore.

Elgar, S., Raubenheimer, B., 2020. Field evidence of inverse energy cascades in the surfzone. J. Phys. Oceanogr. 50, 2315–2321. https://doi.org/10.1175/JPO-D-19-0327.1.

Engle, J., 2003. Formulation of a rip current forecasting technique through statistical analysis of rip current-related rescues (Master's thesis). University of Florida, Gainesville, USA.

Floćh, F., Mabiala, G.R., Almar, R., Castelle, B., Hall, N., Du Penhoat, Y., Scott, T., Delacourt, C., 2018. Flash rip statistics from video images. J. Coast. Res. 81, 100–106. https://doi.org/10.2112/SI81-013.1.

Gensini, V.A., Ashley, W.S., 2009. An examination of rip current fatalities in the United States. Nat. Hazards 54, 159–175.

Gourlay, M. R., 1974. Wave set-up and wave generated currents in the lee of a breakwater or headland, in: Coastal Engineering 1974: Proceedings of the Fourteenth International Conference. American Society of Civil Engineers, New York, 1976–1995.

Great Lakes Surf Rescue Project, 2021. Statistics. http://www.glsrp.org/statistics/ Assessed Date: September 8, 2021.

Grinsted, A., Moore, J.C., Jevrejeva, S., 2004. Application of the cross wavelet transform and wavelet coherence to geophysical time series. Nonlinear Process. Geophys. 11, 561–566. https://doi.org/10.5194/npg-11-561-2004

Horta, J., Oliveira, S., Moura, D., Ferreira, Ó., 2018. Nearshore hydrodynamics at pocket beaches with contrasting wave exposure in southern Portugal. Estuar. Coast. Shelf Sci. 204, 40–55. https://doi.org/10.1016/j.ecss.2018.02.018

Houser, C., Lehner, J., Cherry, N., Wernette, P., 2019. Machine learning analysis of lifeguard flag decisions and recorded rescues. Nat. Hazards Earth Syst. Sci. 19(11), 2541–2549. https://doi.org/10.5194/nhess-19-2541-2019

Lascody R., 1998. East central Florida rip current program. Natl Weather Dig. 22, 25–30.

Leatherman, S.P., Leatherman, S.B., 2017. Techniques for Detecting and Measuring Rip Currents. Int. J. Earth. Sci. Geophys. 3:014.

Lin, Y.T., Schuettpelz, C.C., Wu, C.H., Fratta, D., 2009. A combined acoustic and electromagnetic wave-based techniques for bathymetry and subbottom profiling in shallow waters. J. Appl. Geophys. 68, 203–218. https://doi.org/10.1016/j.jappgeo.2008.11.010

Linares, Á., Bechle, A. J., Wu, C. H., 2016. Characterization and assessment of the meteotsunami hazard in northern Lake Michigan. J. Geophys. Res. Oceans. 121(9), 7141–7158. https://doi.org/10.1002/2016JC011979

Linares, Á., Wu, C. H., Anderson, E. J., Chu, P. Y., 2018. Role of meteorologically induced water level oscillations on bottom shear stress in freshwater estuaries in the Great Lakes. J. Geophys. Res. Oceans. 123, 4970–4987.

Linares, Á., Wu, C.H., Bechle, A.J., Anderson, E.J., Kristovich, D.A.R., 2019. Unexpected rip currents induced by a meteotsunami. Sci. Rep. 9, 2105. https://doi.org/10.1038/s41598-019-38716-2

Liu, P.C., Babanin, A. V., 2004. Using wavelet spectrum analysis to resolve breaking events in the wind wave time series. Ann. Geophys. 22, 3335–3345.

Liu, P.C., Schwab, D.J., Bennett, J.R., 1984. Comparison of a Two-Dimensional Wave Prediction Model with Synoptic Measurements in Lake Michigan, J. Phys. Oceanogr. 14 (9): 1514–1518.

Liu, Y., Wu, C.H., 2019. Lifeguarding Operational Camera Kiosk System (LOCKS) for flash rip warning: Development and application. Coast. Eng. 152, 103537. https://doi.org/10.1016/j.coastaleng.2019.103537

Longuet-Higgins, M.S., Stewart, R. w., 1964. Radiation stresses in water waves; a physical discussion, with applications. Deep Sea Res. Oceanogr. Abstr. 11, 529–562. https://doi.org/10.1016/0011-7471(64)90001-4

Lushine, J.B., 1991. A study of rip current drownings and related weather factors. Natl. Weather Dig. 16, 13-19.

MacMahan, J. H., Thornton, E. B., Reniers, A. J. H. M., 2006. Rip current review. Coast. Eng. 53, 191–208. https://doi.org/10.1016/J.COASTALENG.2005.10.009.

MacMahan, J. H., Reniers, A. J. H. M., Thornton, E.B., 2010. Vortical surf zone velocity fluctuations with 0(10) min period. J. Geophys. Res. 115, C06007. https://doi.org/10.1029/2009JC005383

McCarroll, R.J., Brander, R.W., Turner, I.L., Power, H.E., Mortlock, T.E., 2014. Lagrangian observations and circulation on an embayed beach with headland rip currents. Mar. Geol. 355, 173–188.

Meadows, G., Purcell, H., Guenther, D., Meadows, L., Kinnunen, R.E., Clark, G., 2011. Rip Currents in the Great Lakes: An Unfortunate Truth, in: Leatherman, S., Fletemeyer, J. (Eds.), Rip Currents: Beach Safety, Physical Oceanography, and Wave Modeling. CRC Press, Boca Raton, 199–214.

Michigan Sea Grant, 2021. Great Lakes Current Incident Database. https://www.michiganseagrant.org/dcd/dcdsearch.php. Assessed date: September 8, 2021.

Monserrat, S., Vilibić, I., Rabinovich, A.B., 2006. Meteotsunamis: atmospherically induced destructive ocean waves in the tsunami frequency band. Nat. Hazards Earth Syst. Sci. 6, 1035–1051. https://doi.org/10.5194/nhess-6-1035-2006

Moulton, M., Dusek, G., Elgar, S., Raubenheimer, B., Moulton, M., Dusek, G., et al., 2017. Comparison of rip current hazard likelihood forecasts with observed rip current speeds. Wea. Forecasting. 32 (4), 1659–1666. https://doi.org/10.1175/WAF-D-17-0076.1

Murray, T., Cartwright, N., Tomlinson, R., 2013. Video-imaging of transient rip currents on the Gold Coast open beaches. J. Coast. Res. 165, 1809–1814. https://doi.org/10. 2112/SI65-306.1.

National Geophysical Data Center, 1996. Bathymetry of Lake Michigan. National Geophysical Data Center, NOAA. doi:10.7289/V5B85627. Accessed date: December 9, 2019

National Weather Service, NOAA, 2020. 2020 Lake Michigan Beach Forecast Services - Will You be Safe from Dangerous Swimming Conditions this Year? https://www.weather.gov/mkx/beachhazardprogram. Accessed date: 31 July 2020.

Nortek AS, 2005. AWAC: Acoustic Wave and Current Meter, User Guide, N3000-126, Revision E, Norway.

Office for Coastal Management, 2014. Coastal Topobathy Lidar. https://www.coast.noaa.gov/digitalcoast/data/jalbtcx.html. Assessed date: December 9, 2019

Pattiaratchi, C., Olsson, D., Hetzel, Y., Lowe, R., 2009. Wave-driven circulation patterns in the lee of groynes. Cont. Shelf Res. 29, 1961–1974.

Rabinovich, A. B., 2009. Seiches and harbor oscillations, in: Kim, Y.C. (Ed.), Handbook of Coastal and Ocean Engineering. World Scientific Publishing Company, Toh Tuck Link,Singapore, 193–236.

Reimer, J. R., Wu, C. H., 2016. Development and Application of a Nowcast and Forecast System Tool for Planning and Managing a River Chain of Lakes. Water Resour. Manag. 30, 1375–1393. https://doi.org/10.1007/s11269-016-1228-7

Schrader, M., 2004. Evaluation of the modified ECFL LURCS rip current forecasting scale and conditions of selected rip current events in Florida (Master's thesis). University of Florida, Gainesville, USA.

Schwab, D.J., Bennett, J.R., Lynn, E.W., 1984. A Two-dimensional Lake Wave Prediction System, TM-051.

Scott, T., Austin, M., Masselink, G., Russell, P., 2016. Dynamics of rip currents associated with groynes — field measurements, modelling and implications for beach safety. Coast. Eng. 107, 53–69.

Shepard, F.P., 1936. Undertow, rip tide or "rip current". Science. 84, 181–182.

Shi, F., Svendsen, I.A., Kirby, J.T., McKee Smith, J., 2003. A curvilinear version of a quasi-3D nearshore circulation model. Coast. Eng. 49 (1–2), 99–124.

Short, A.D., Hogan, C.L., 1994. Rip currents and beach hazards, their impact on public safety and implications for coastal management. J. Coast. Res. Special Issue 12 on Coastal Hazards: Perception, Susceptibility and Mitigation, 197–209.

Torrence, C., Compo, G.P., 1998. A practical guide to wavelet analysis, Bull. Am. Meteorol. Soc., 79, 61–78.

Wanek, J. M., Wu, C. H., 2006. Automated trinocular stereo imaging system for three-dimensional surface wave measurements. Ocean Eng. 33, 723–747.

Wind, H.G., Vreugdenhil, C.B., 1986. Rip-current generation near structures. J. Fluid Mech. 171, 459–476.

Woodward, E., Beaumont, E., Russell, P., Wooler, A., Macleod, R., 2013. Analysis of rip current incidents and victim demographics in the UK. J. Coast. Res. 65 (Special Issue 1), 850–855.

van Rijn, L.C., 2011. Coastal erosion and control. Ocean Coast. Manag. 54 (12), 867–887. https://doi.org/10.1016/j.ocecoaman.2011.05.004

Figure captions

Fig.1. Map of the study site at Port Washington, WI (abbreviated as PW). Color contours show the nearshore bathymetry. Locations of observation stations and field measurement sensors are depicted in markers denoted with specific letters and numbers. A1 is NDBC meteorology station (PWAW3). A2 is the real-time camera and the weather station. C1, C2 are up-looking ADCPs deployed on the north side of the north breakwater; CW is an AWAC and W1 is an Echologger that were deployed near the North Beach. KMKE is ASOS station at Milwaukee.

Fig. 2. Time series of current speeds and directions measured at three locations of (a) C1, (b) C2, and (c) CW during the field measurements from 2016/07/27 to 2016/08/31. Gray lines represent the rip identification thresholds for speeds (dashed line) and directions (solid lines). A total of fourteen rip current events are highlighted in shaded rectangles and labeled chronologically from 1 to 14 with a letter of *I* or *D* to denote forms of increasing or decreasing speeds from C1 to C2.

Fig. 3. Wavelet power spectra (WPS, in log scale) of current speeds at three locations of (a) C1, (b) C2, and (c) CW during the fourteen identified rip current events. WPS were normalized against the variance. Black solid contours represent the 95% confidence level.

Fig. 4. Time series of environmental conditions from 2016/07/27 to 2016/08/31 for (a) nearshore wave significant height (H_s), peak wave period (T_p) measured at CW; (b) surface wind speeds (W_s) and directions (Dir_w) at A1; (c) high-pass filtered water level fluctuations (ΔWL) at CW; and (d) high-pass filter atmospheric pressure disturbances (ΔP) at A1.

Fig. 5. Cross-wavelet power spectra (CWPS) of current velocities measured at C2 (Vel) and (a) water levels (WL) at CW, (b) atmospheric pressures (P) at A1, and (c) wind speeds (W_s) at A1. The x axis tick spacing represents a 1-hour interval. The CWPS were normalized by the 95% confidence level (power relative to significant level) and black solid contours represent CWPS that are statistically significant at the $\alpha = 5\%$ level.

Fig. 6. Examples of camera images viewing toward the north breakwater at Port Washington, WI during events: (a) event 1 on 2016/07/29 at 12:16, (b) event 3 on 2016/07/30 at 19:01, (c) event 9 on 2016/08/20 at 10:17, (d) event 5 on 2016/08/12 at 09:17. For events 1, 3, and 9 in (a-c), visual signatures of sediment plumes induced by rip currents and longshore feeding currents, highlighted in red arrows, were visually evident.

Fig. 7. A webpage display for providing real-time assessments of potential occurrences of rip currents near the north breakwater at Port Washington, WI. A rip current event on 2019/08/15, as an example, was assessed to be in the *high*-risk tier with a total point of 10.5 using the SRiCAM. Current conditions of the nine factors, a real-time webcam image, and safety messages are displayed on the webpage.

Fig. 8. (a) Assessment of rip current potential occurrences on July 20, 2019 at 39 locations near harbor breakwaters in Lake Michigan. (b-d) images with sediment plume signatures (marked as red arrows) obtained from the three webcams at sites [1] Port Washington (on the west coast of Lake Michigan), [14] Michigan City, IN (on the south coast), and [21] Grand Haven, MI (on the east coast). (e) An image without sediment plume signature at site [17] South Haven, MI.

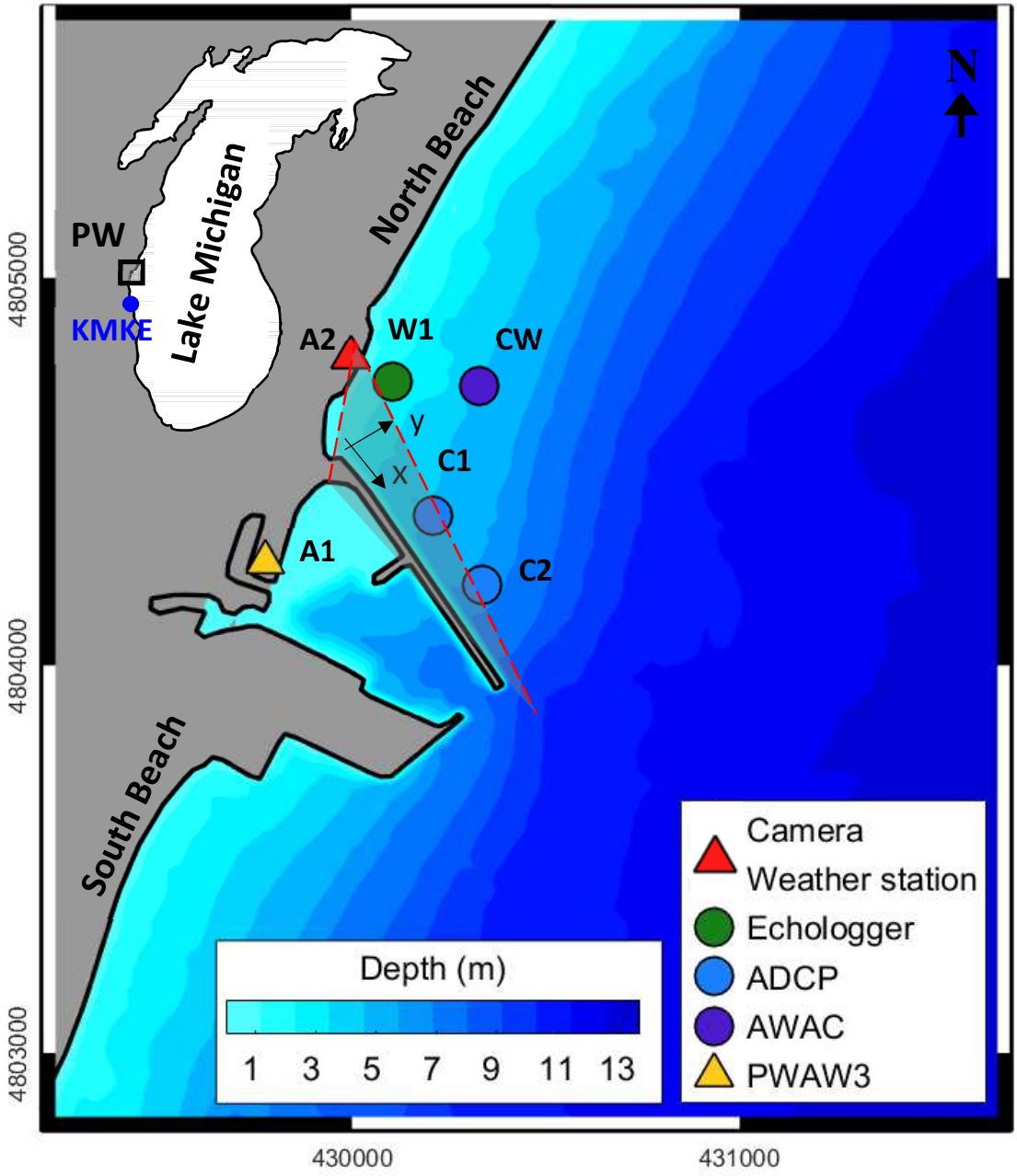
N
North Beach
Lake Michigan
PW
KMKE
A2
W1
CW
y
x
C1
A1
C2
South Beach
Depth (m)
1 3 5 7 9 11 13
Camera
Weather station
Echologger
ADCP
AWAC
PWAW3
4805000
4804000
4803000
430000
431000

Fig.1.

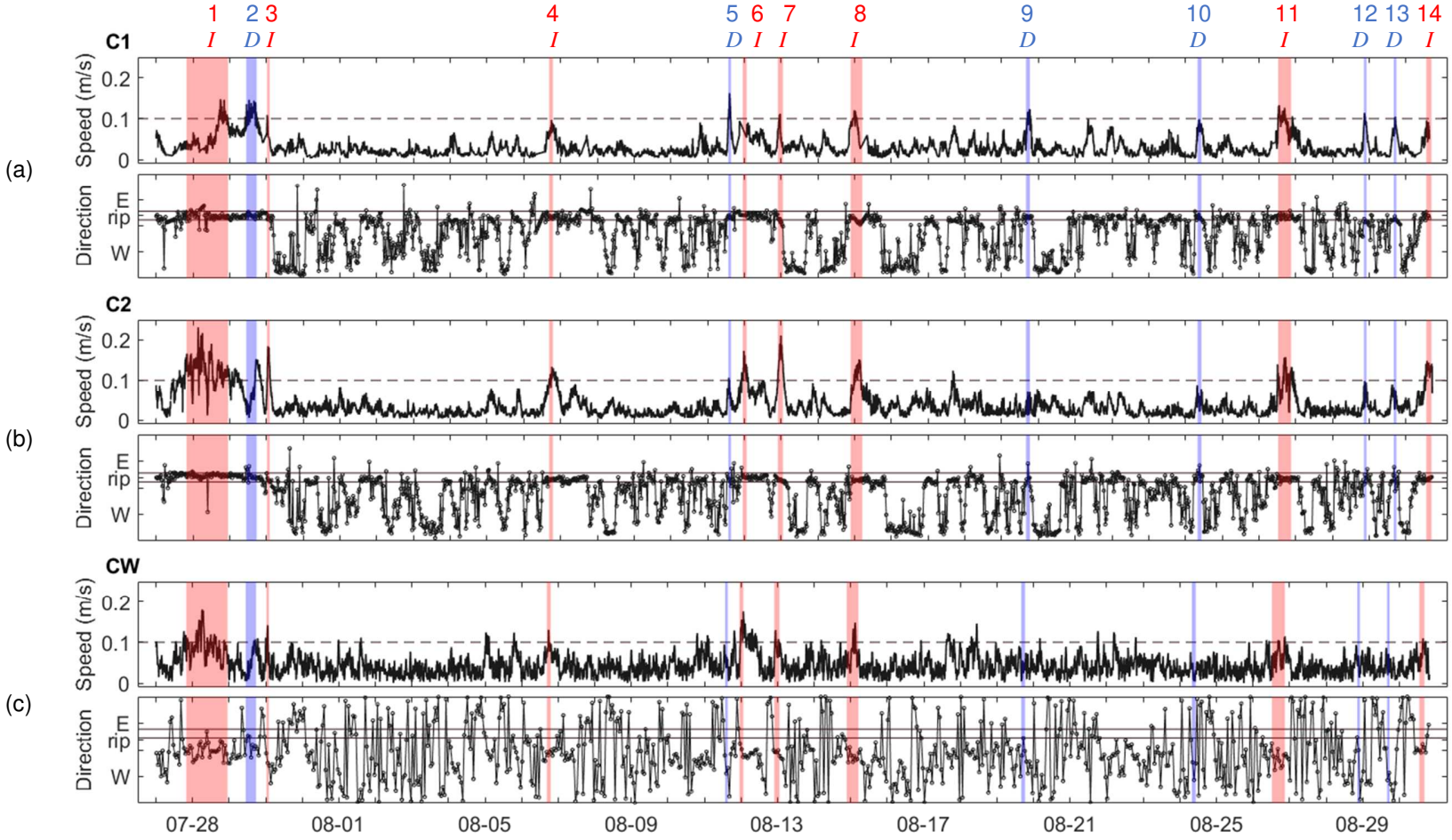
1 2 3 4 5 6 7 8 9 10 11 12 13 14
I D I I D I I I D D I D D I
(a)
C1
Speed (m/s)
0.2
0.1
0
Direction
E
nip
W
(b)
C2
Speed (m/s)
0.2
0.1
0
Direction
E
nip
W
(c)
CW
Speed (m/s)
0.2
0.1
0
Direction
E
nip
W
07-28
08-01
08-05
08-09
08-13
08-17
08-21
08-25
08-29

Fig. 2.

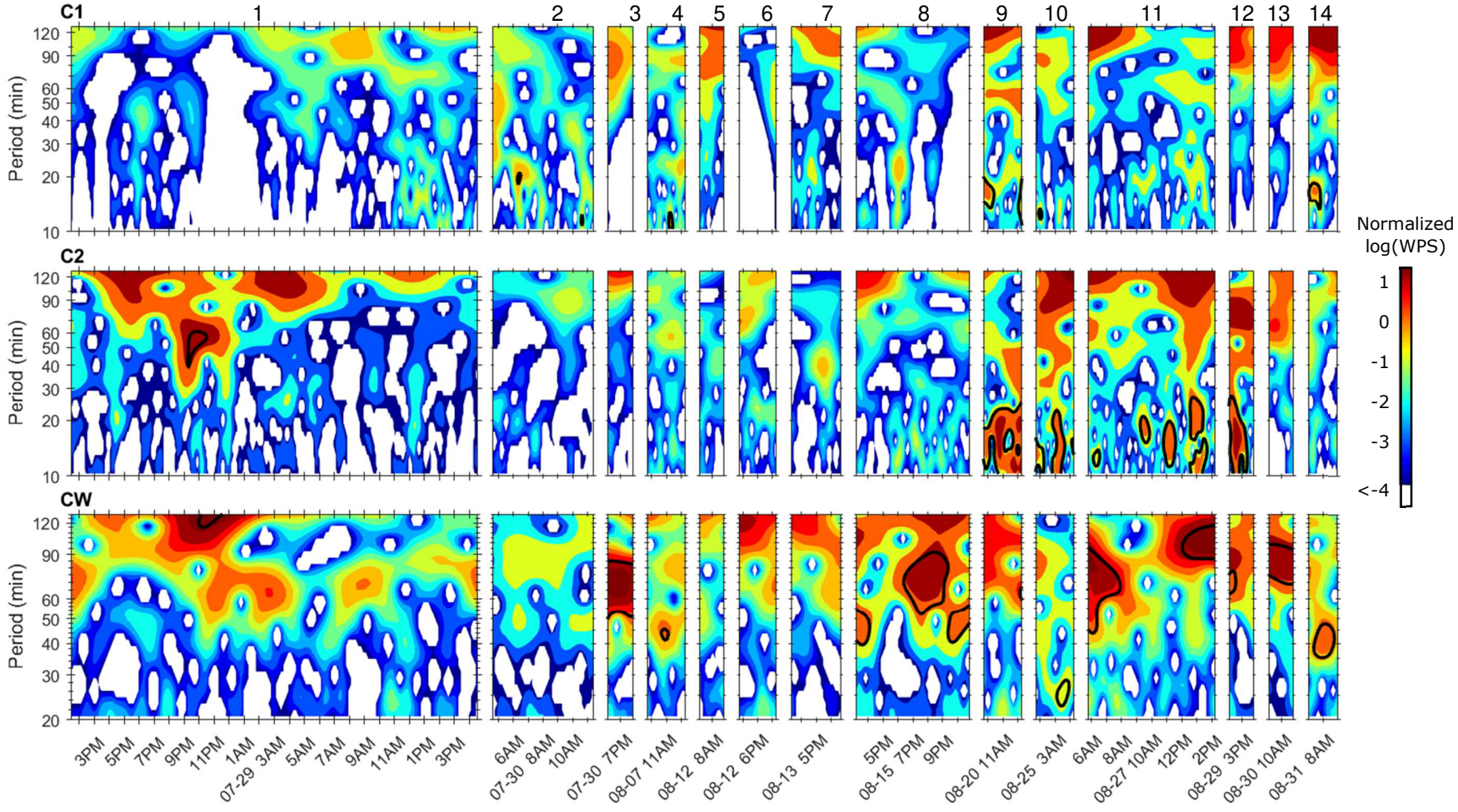
C1
C2
CW
Period (min)
120
90
60
50
40
30
20
10
1
2
3
4
5
6
7
8
9
10
11
12
13
14
3PM
5PM
7PM
9PM
11PM
1AM
07-29 3AM
5AM
7AM
9AM
11AM
1PM
3PM
6AM
07-30 8AM
10AM
07-30 7PM
08-07 11AM
08-12 8AM
08-12 6PM
08-13 5PM
5PM
08-15 7PM
9PM
08-20 11AM
08-25 3AM
6AM
8AM
08-27 10AM
12PM
2PM
08-29 3PM
08-30 10AM
08-31 8AM
Normalized log(WPS)
1
0
-1
-2
-3
<-4

Fig. 3.

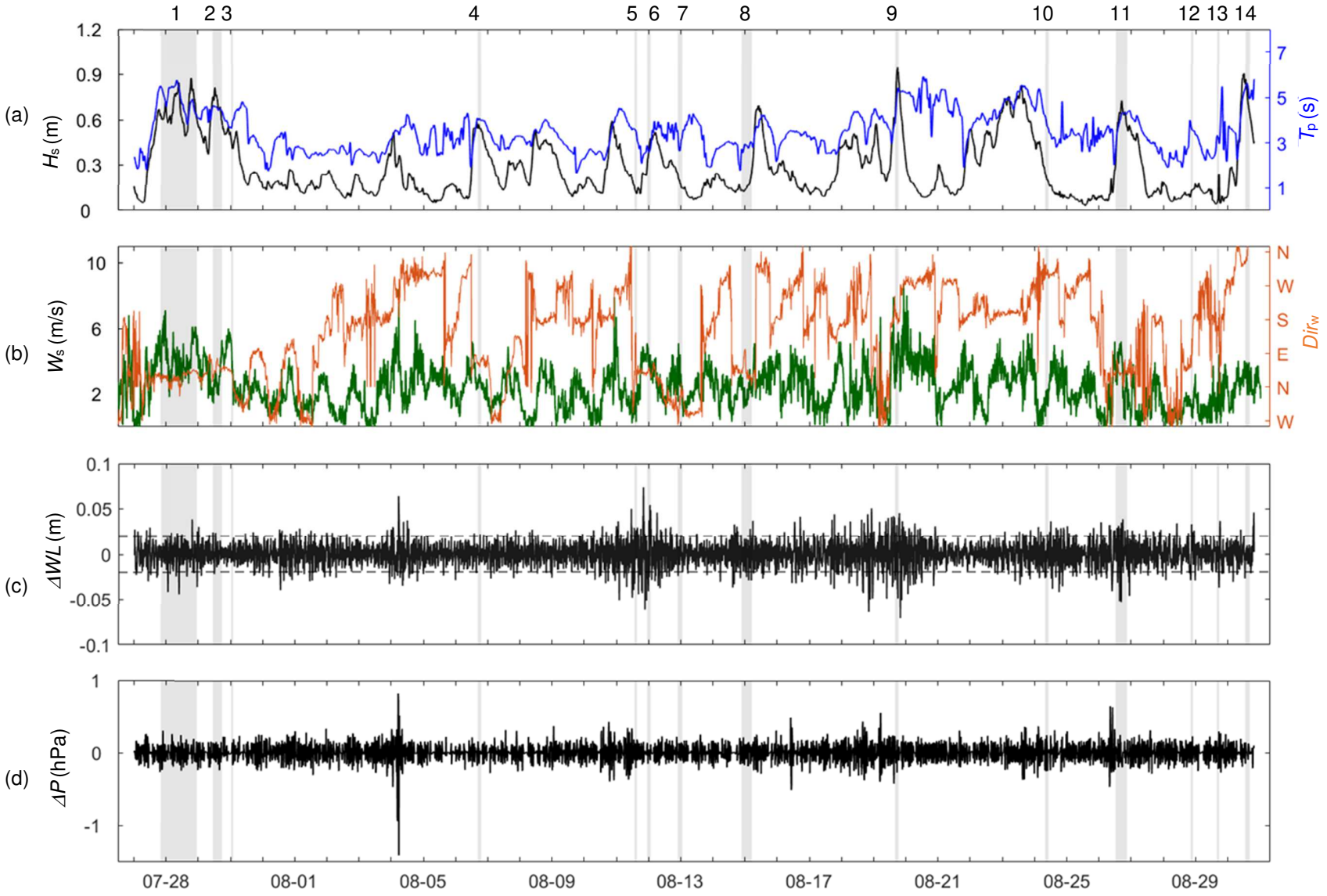
1 2 3 4 5 6 7 8 9 10 11 12 13 14
(a)
H_s (m)
T_p (s)
(b)
W_s (m/s)
Dir_w
N W S E N W
(c)
ΔWL (m)
(d)
ΔP (hPa)
07-28 08-01 08-05 08-09 08-13 08-17 08-21 08-25 08-29

Fig. 4.

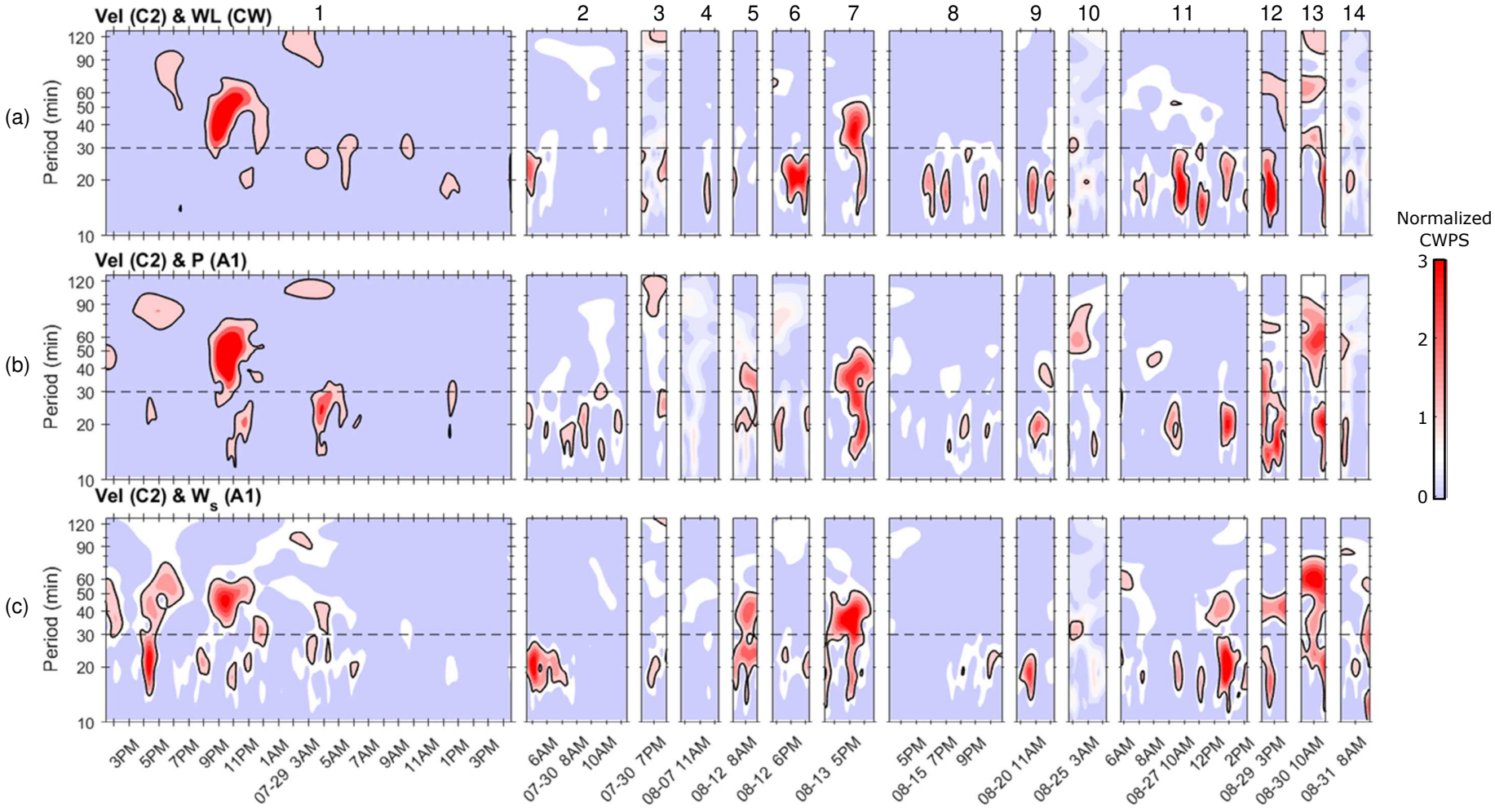
Vel (C2) & WL (CW)
Vel (C2) & P (A1)
Vel (C2) & W$_s$ (A1)
(a)
(b)
(c)
Period (min)
120
90
60
50
40
30
20
10
1
2
3
4
5
6
7
8
9
10
11
12
13
14
3PM
5PM
7PM
9PM
11PM
1AM
07-29 3AM
5AM
7AM
9AM
11AM
1PM
3PM
6AM
07-30 8AM
10AM
07-30 7PM
08-07 11AM
08-12 8AM
08-12 6PM
08-13 5PM
5PM
08-15 7PM
9PM
08-20 11AM
08-25 3AM
6AM
8AM
08-27 10AM
12PM
2PM
08-29 3PM
08-30 10AM
08-31 8AM
Normalized CWPS
3
2
1
0

Fig. 5.

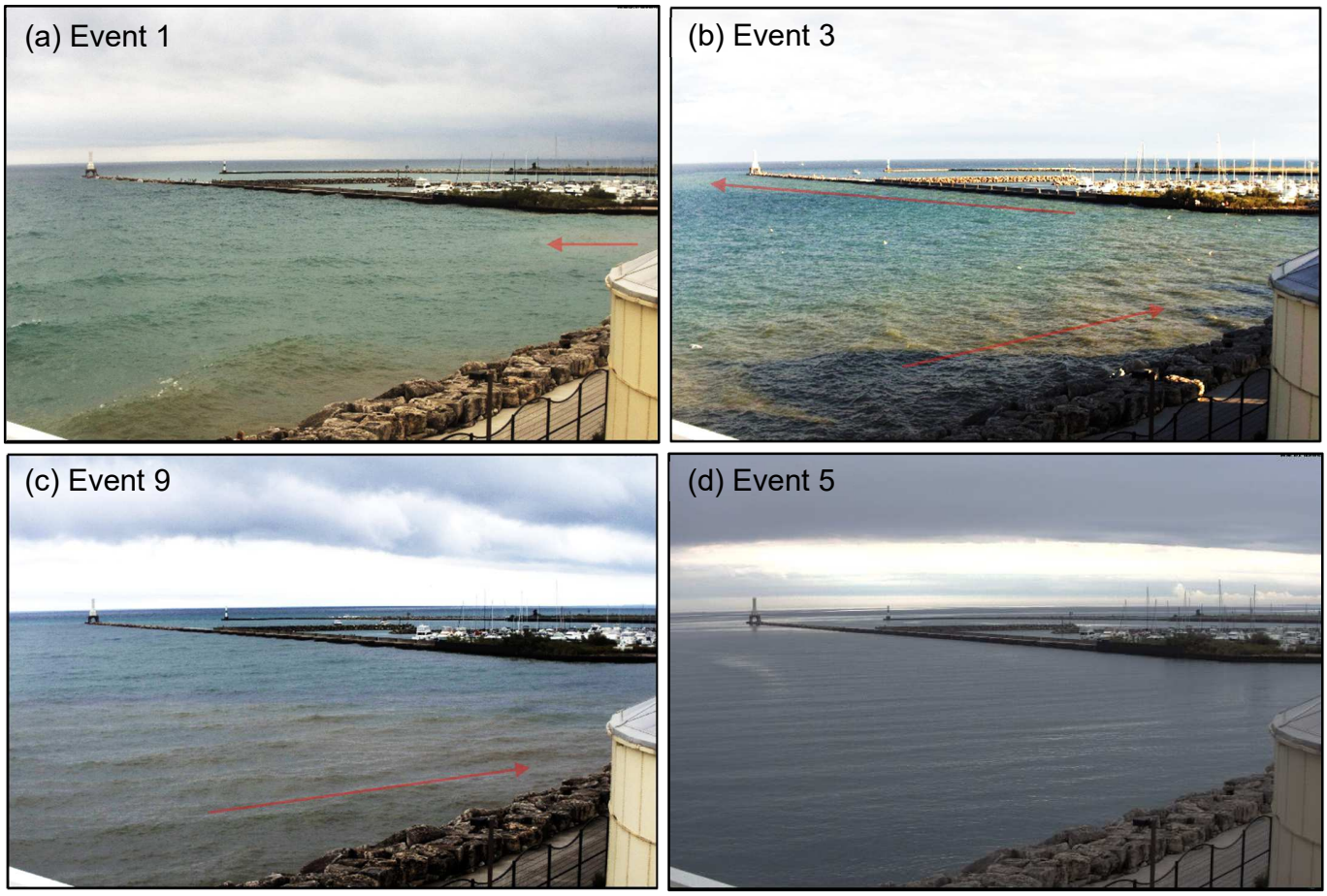

Fig. 6.

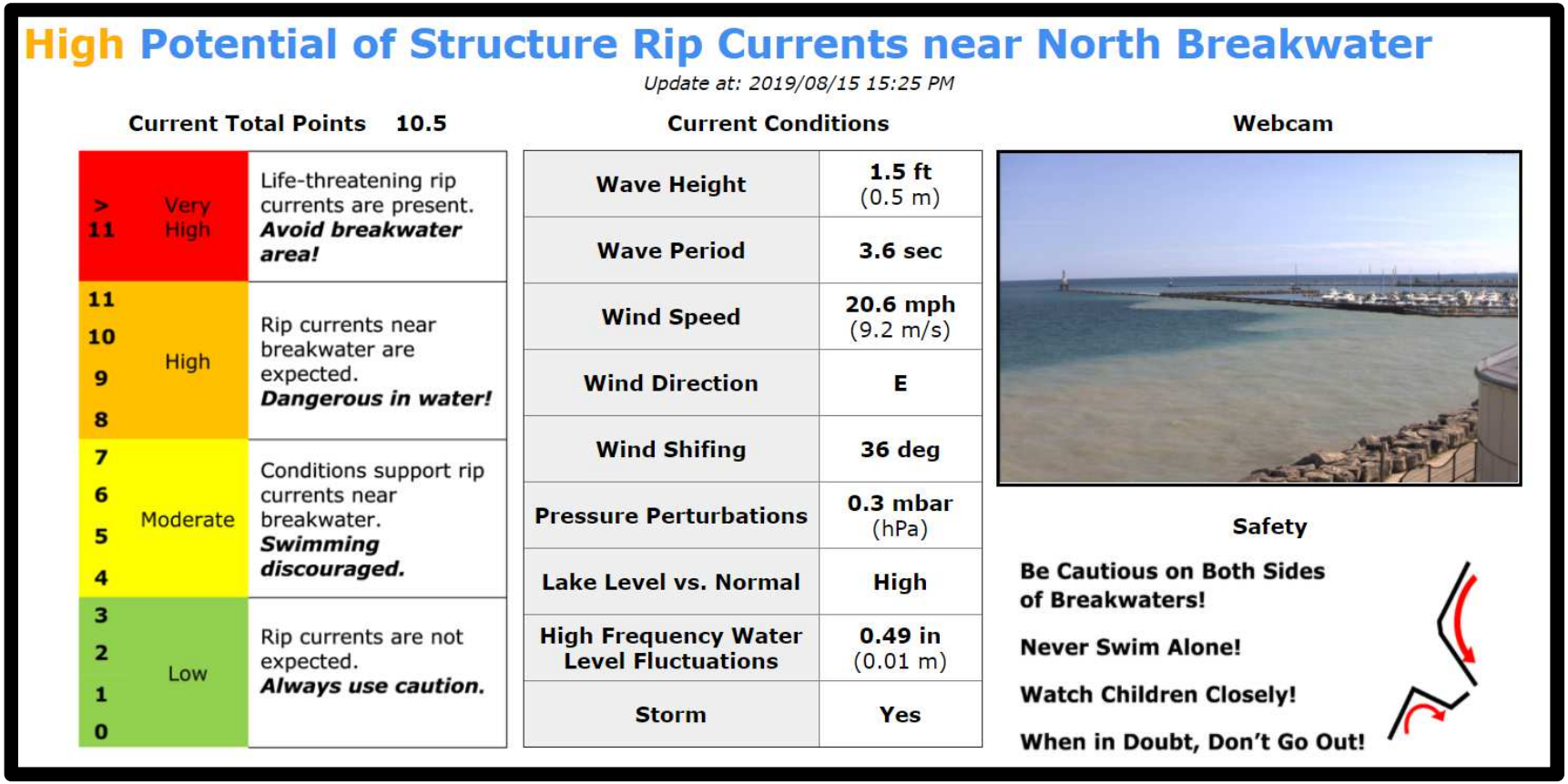
High Potential of Structure Rip Currents near North Breakwater
Update at: 2019/08/15 15:25 PM
Current Total Points 10.5
> 11 Very High
Life-threatening rip currents are present. Avoid breakwater area!
11 10 9 8 High
Rip currents near breakwater are expected. Dangerous in water!
7 6 5 4 Moderate
Conditions support rip currents near breakwater. Swimming discouraged.
3 2 1 0 Low
Rip currents are not expected. Always use caution.
Current Conditions
Wave Height 1.5 ft (0.5 m)
Wave Period 3.6 sec
Wind Speed 20.6 mph (9.2 m/s)
Wind Direction E
Wind Shifing 36 deg
Pressure Perturbations 0.3 mbar (hPa)
Lake Level vs. Normal High
High Frequency Water Level Fluctuations 0.49 in (0.01 m)
Storm Yes
Webcam
Safety
Be Cautious on Both Sides of Breakwaters!
Never Swim Alone!
Watch Children Closely!
When in Doubt, Don't Go Out!

Fig. 7.

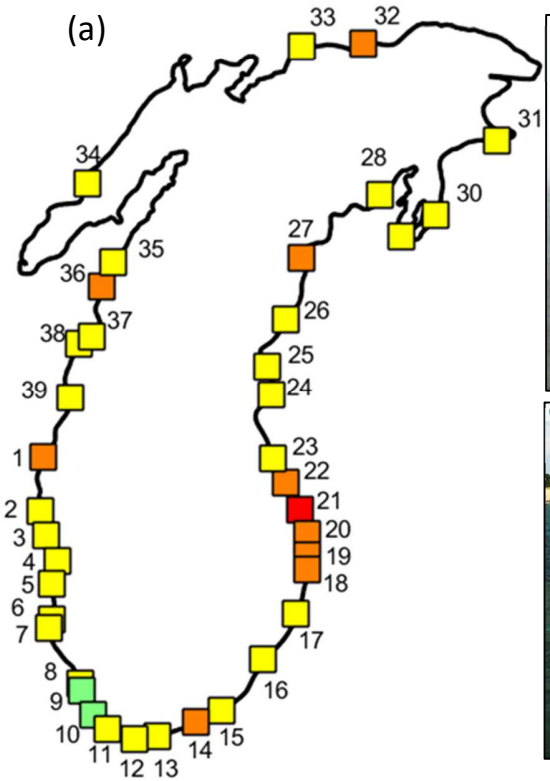

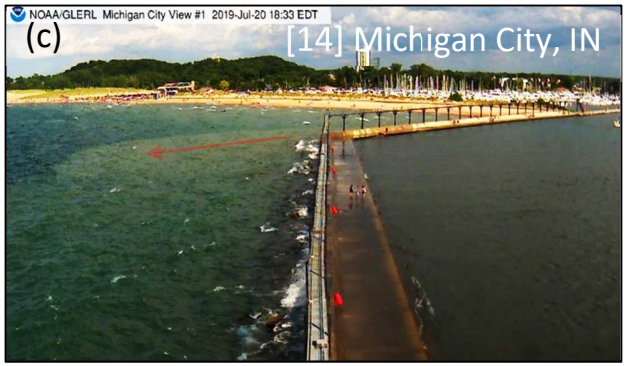

	Site	Points	[10]	South Chicago, IL	3.5	[20]	Port Sheldon, MI	9.5	[30]	Elk Rapids, MI	4.5
[1]	Port Washington, WI	10.5	[11]	Calumet Harbor, IL	4	[21]	Grand Haven, MI	11.5	[31]	Bay Harbor, MI	5.5
[2]	Milwaukee, WI	5	[12]	Gary, IN	6	[22]	Muskegon, MI	7.5	[32]	Port Inland, MI	8
[3]	South Milwaukee, WI	4	[13]	Burns Harbor, IN	6	[23]	Wabaningo, MI	6.5	[33]	Manistique, MI	7
[4]	Racine, WI	5.5	[14]	Michigan City, IN	9	[24]	Pentwater, MI	4.5	[34]	Menominee, MI	6
[5]	Kenosha, WI	5.5	[15]	New Buffalo, MI	6	[25]	Ludington, MI	6.5	[35]	Algoma, WI	5.5
[6]	Waukegan, IL	4.5	[16]	St. Joseph, MI	7	[26]	Manistee, MI	5.5	[36]	Kewaunee, WI	7.5
[7]	North Chicago, IL	4.5	[17]	South Haven, MI	6.5	[27]	Frankfort, MI	8	[37]	Two Rivers, WI	6
[8]	Sheridan Park, IL	5	[18]	Saugatuck Dunes, MI	8.5	[28]	Leland, MI	7	[38]	Manitowoc, WI	6.5
[9]	Chicago, IL	2	[19]	Holland, MI	9	[29]	Traverse City, MI	6.5	[39]	Sheboygan, WI	5.5

Figure 8.

Table 1. Structure Rip Checklist and Assessment Matrix (SRiCAM).

Wave Height		Point
1 ft	(0.3 m)	0.5
2 ft	(0.6 m)	1
3-4 ft	(0.9-1.2 m)	2
5-7 ft	(1.5-2.1 m)	3
8-10 ft	(2.4 -3.0 m)	4
>10 ft	(3.0 m)	5

Wave Factor _____

Wave Period	Point
3-4 sec	0.5
4-5 sec	1
5-6 sec	2
> 6 sec	3

Period Factor _____

Wind Direction	Point
downdrift	1
updrift	2

Direction Factor _____

Wind Shift	Point
>15 deg/hr	1

Wind Shifting Factor _____

Pressure Disturbance	Point
> 0.5 hPa	1

Pressure Factor _____

Wind Speed		Point
0-5 kt	(0-2.6 m/s)	0.5
6-8 kt	(3.1-4.1 m/s)	1
9-11 kt	(4.6-5.7 m/s)	1.5
12-14 kt	(6.2-7.2 m/s)	2
15-17 kt	(7.7-8.7 m/s)	3
18-20 kt	(9.3-10.3 m/s)	4
>20 kt	(10.3 m/s)	5

Wind Factor _____

Lake Level vs Normal		Point
> 3 in	(0.08 m)	-0.5
normal		0
-6 to -10 in	(0.15.2-0.25 m)	1
> -11 in	(0.28m)	2

Lake level Factor _____

High Frequency Water Level Fluctuations		Point
1.5 to 3 in	(0.04-0.08 m)	0.5
>3 in	(0.08 m)	1

HFWLO Factor _____

Visual Image	Point
Storm structure	1
Sediment plume	4

Visual Factor _____

Total Points (TP) _____

TP<4	4 ≤ TP ≤ 7	7 < TP ≤11	TP >11
Low	Moderate	High	Very High

Table 2. Summary of rip current events identified during 2016 field measurements and associated environmental conditions.

	Events in 2016	**Currents**			**Proxies**	**Waves**		**Water Level Changes**	**Wind & Pressure Disturbances**				**Storms**
#	Date & time	Form	U_{max} (m/s)	ΔT (hr)		H_s (m)	T_p (sec)	ΔWL (m)	W_s (m/s)	Dir_w (from)	ΔDir_w (°/hr)	ΔP (hPa)	
1	07/28 14:00 – 07/29 17:00	*I*	0.23	27.1	I,V,VI,VII	0.67	4.9	0.08	7.1	NE	0	0.57	cluster
2	07/30 05:00 – 07/30 13:30	*D*	0.15	8.5	I,V,VII	0.72	4.5	0.05	5.1	NE	3	0.39	cluster
3	07/30 18:35 – 07/30 20:20	*I*	0.18	1.7	II,VII	0.43	3.8	0.03	5.2	NE	22	0.46	cluster
4	08/07 10:40 – 08/07 13:15	*I*	0.13	2.5	I	0.55	4.0	0.03	3.2	ENE	1	0.45	none
5	08/12 07:45 – 08/12 09:30	*D*	0.16	1.7	IV,V,VI,VII	0.12	3.5	0.04	2.1	ENE	15	0.71	linear
6	08/12 17:05 – 08/12 19:35	*I*	0.17	2.5	II,V,VI,VII	0.40	2.7	0.10	5	NE	4	0.57	linear
7	08/13 16:00 – 08/13 19:25	*I*	0.21	3.4	II,V	0.18	3.0	0.05	5.1	NNW	17	0.38	none
8	08/15 15:30 – 08/15 23:10	*I*	0.15	7.6	II,V,VII	0.16	2.8	0.06	3.5	NE	6	0.41	complex
9	08/20 10:05 – 08/20 12:35	*D*	0.12	2.5	III,V,VI, VII	0.84	4.9	0.08	5.8	S	2	0.98	bow
10	08/25 02:00 – 08/25 04:35	*D*	0.10	2.5	II,V,VI, VII	0.21	3.9	0.05	2.3	NE	0	0.71	cluster
11	08/27 06:40 – 08/27 15:05	*I*	0.16	8.5	I,V,VI,VII	0.61	4.0	0.09	5.2	NE	2	1.12	complex
12	08/29 14:35 – 08/29 16:20	*D*	0.11	1.7	IV,V	0.13	3.6	0.06	1.4	E	36	0.43	none
13	08/30 10:10 – 08/30 11:50	*D*	0.10	1.7	IV,VI	0.12	3.3	0.03	4.4	SSE	25	0.52	none
14	08/31 07:20 – 08/31 10:45	*I*	0.15	3.4	I	0.76	5.4	0.02	3.9	N	22	0.39	none

Table 3. Validation of the SRiCAM for rip current events identified near the north breakwater at Port Washington, WI.

#	Rip Current Events (2016-2019)	Velocity	Image	Total Points	Assessment	Contribution from New Factors
1	7/29/2016 03:30	yes	yes	12.5	*very high*	72%
2	7/30/2016 08:25	yes	yes	10.5	*high*	71%
3	7/30/2016 19:25	yes	yes	10.5	*high*	81%
4	8/07/2016 12:00	yes		4.5	*moderate*	56%
5	8/12/2016 08:35	yes		5.5	*moderate*	91%
6	8/12/2016 18:25	yes		6.5	*moderate*	77%
7	8/13/2016 17:40	yes		4.5	*moderate*	78%
8	8/15/2016 19:20	yes		4	*moderate*	88%
9	8/20/2016 11:20	yes	yes	11	*high*	73%
10	8/25/2016 03:20	yes		5	*moderate*	90%
11	8/27/2016 10:50	yes		7	*moderate*	71%
12	8/29/2016 15:30	yes		4	*moderate*	88%
13	8/30/2016 11:00	yes		4.5	*moderate*	78%
14	8/31/2016 09:00	yes		7	*moderate*	50%
15	8/11/2017 01:05	yes		6.5	*moderate*	77%
16	8/15/2017 12:05	yes	yes	11.5	*very high*	78%
17	8/16/2017 22:25	yes		6	*moderate*	83%
18	8/17/2017 09:05	yes	yes	12	*very high*	75%
19	8/17/2017 14:55	yes		9	*high*	56%
20	8/17/2018 10:10		yes	11.5	*very high*	70%
21	6/28/2019 08:15		yes	12.5	*very high*	72%
22	8/15/2019 15:25		yes	10.5	*high*	95%